3D Shape Analysis for Liver-Gallbladder Anatomical Structure Retrieval

Weimin Huang[1], Wei Xiong[1], Jiayin Zhou[1], Jing Zhang[5], Tao Yang[1], Jiang Liu[1], Yi Su[2], Calvin Lim[2], Chee Kong Chui[3], and Stephen Chang[4]

[1] Institute for Infocomm Research, Agency for Science, Technology and Research, 1 Fusionopolis Way, #21-01 Connexis South Tower, Singapore 138632, Singapore
{wmhuang,wxiong,jzhou,tyang,jliu}@i2r.a-star.edu.sg
[2] Institute of High Performance Computing, Agency for Science, Technology and Research, 1 Fusionopolis Way, #16-16 Connexis North Tower, Singapore 138632, Singapore
{suyi,limcw}@ihpc.a-star.edu.sg
[3] Department of Mechanical Engineering, Faculty of Engineering, National University of Singapore, Centre for Biomedical Materials Application and Technology, 9 Engineering Drive 1, Singapore 117576, Singapore
mpecck@nus.edu.sg
[4] Department of Surgery, National University Hospital, 1E Kent Ridge Road, Singapore 119228, Singapore
cfscky@nus.edu.sg
[5] Department of Medical Information Engineering, School of Electrical Engineering and Information, Sichuan University, P.R. China
dzzj2001@gmail.com

Abstract. Anatomical structure is important for medical education and disease diagnosis. In the application of surgical simulation, different anatomical structures can be retrieved to create variety of surgical scenarios for training, while similar structures can also be retrieved to assist disease diagnosis. This paper presents an approach to liver-gallbladder anatomical structure retrieval with 3D shape comparison, where the direct shape comparison based on dense shape registration is applied to liver shape due to its shape complexity, and feature based comparison is applied to gallbladder shape with a semantic shape decomposition using the saliency area based on multi-scale curvatures and concavity. After the registration of liver models, the geometric structure of the gallbladder and liver can be combined for joint comparison. With the 3D models constructed from a set of liver-gallbladder CT data, experiments are conducted for joint liver-gallbladder retrieval. Encouraging result shows that it can reveal important topology based on similarity and variance of 3D shapes and has a similar performance compared to that of manual retrieval by human operators.

Keywords: Anatomical structure, shape analysis, shape comparison, surgical simulation.

1 Introduction

Anatomical relationships of liver and gallbladder (GB), of which some are rare such as the left GB and intrahepatic GB, may pose challenges to the surgeons. The GB

H. Yoshida, D. Hawkes, M.W. Vannier (Eds.): Abdominal Imaging 2012, LNCS 7601, pp. 178–187, 2012.

shape information, such as extra large size of a GB or folds on a GB, is not only useful for surgery and training, but may also reveal some potential pathological risks. In laparoscopic surgery and simulation of cholecystectomy, anatomical shape and structure of the liver and GB, including the position, size and wall thickness, are some of the important factors that affect the difficulty of such surgeries. Most of the current surgery simulation systems mainly aim at the training on fundamental laparoscopic skills (FLS) with generic liver, GB and other organ models. Such a simulation thus lacks the facility to supply different scenarios with different challenges for training. However it is possible to construct new models from patient CT data and store the models in a model library for future training as well as patient specific surgery planning and preoperative practice.

The training with new models can assist the surgeon trainees by exposing them with new scenarios and different challenges instead of a single generic model. With increasing number of models, it becomes difficult for a trainee to select suitable training cases, to cater for his/her specific training purposes. Thus a reliable approach to compare and retrieve the relevant (similar or dissimilar) anatomical structure is highly needed.

1.1 Related Works

GB diseases have varying symptoms, which sometimes can be shown in the shape change of a GB [1, 2]. Although the shape anomaly may not always be related to disease, it may cause the stasis that could lead to stone formation and inflammation [3]. Measurement for wall thickness from CT images has been studied by Prasad *et al* [4]. Noticeably, GBs can also vary from person to person in terms of size, shape and location, which pose the challenges for new surgeons.

In cholecystectomy, liver is the main surrounding organ of GB. Thus liver shape is to be modeled in the simulation and the anatomical relationship specifies the surgery scenario. In the literature, liver shape model has been successfully applied for atlas construction [5] and segmentation [6]. However there is no study on the retrieval of anatomical structure of liver-GB. The statistical liver shape model and liver shape retrieval has been successfully applied for segmentation [7]. However there is no systematic study on the retrieval of liver-gallbladder. Work in [8] presented physics modeling of GB, which did not address GB shape analysis. In [9] the researchers described an approach to a 3D shape decomposition, which is improved using a more robust saliency method in this paper.

In 3D model retrieval, works include shape description, modeling and similarity measurement [10]. Generally a 3D shape can be represented by tetrahedral or polyhedral mesh. Focusing on surface model, there are three main categories of 3D shape analysis. One is based on the mesh patch segmentation from the salient points on the surface [11], and the second is based on skeletonization of 3D shapes or logical parts decomposition [12]. Besides, there are some works proposed to compare the shape based on the registered models directly using the distance of the corresponding points [13, 14]. To segment an object into meaningful parts, minima rule and part salience [15] have been proposed. Banegas *et al* presented a decomposition of volume data

[16], and then ellipsoids are fitted and deformed to reconstruct the object from the hierarchical decomposition.

1.2 Contributions

This paper presents an approach to the application in joint liver-GB shape comparison and retrieval, where direct shape registration and comparison based on Coherent Point Drift (CPD) [13] is adopted to compute liver shape similarity and semantic features are proposed for GB shape comparison. Using CPD is due to its speed and nonlinearity for non-rigid shape registration. Combining the distance measurement of the liver-GB anatomical structures, users can retrieve the similar or dissimilar data sets for surgery training or pathological comparisons. Noted that the liver-gallbladder pairs are essentially in a continuous shape space, as no categories are defined for joint liver-gallbladder anatomical structure, the conventional precision-recall measurement can not be adopted for the retrieval performance evaluation. Instead, the Spearman's score for rank correlation [20] is used to compare the order of the retrieval data sets with the result from human operators, which can be the trainee surgeons or technicians who are selecting similar or dissimilar anatomical structures for training.

2 Liver-Gallbladder Model Comparison

The preprocessing of CT data to reconstruct liver and GB model is based on our previous work for CT image segmentation and mesh construction and optimization [17], [18]. This paper focuses on liver-GB shape analysis and retrieval, where we compare liver shape based on direct shape distance due to the complexity of liver shape, while model GBs with meaningful semantic features.

2.1 Similarity of Liver Shapes

The registration method adopted here is based on CPD where point set registration is formulated as a probability density estimation problem. The moving set is modeled by a Gaussion mixture model (GMM) with unknown centroids. It forces the GMM centroids to move coherently as a group by reparameterizing the centroid locations explicitly. The form of transformation is non-rigid. Since we choose to use a fast Gaussian transformation [13] the registration is fast (about 10 seconds for 2 sets of 1000 points/vertices on surface mesh). Given the registration of liver shapes L_1 and L_2, we compute the mean Hausdorff distance of the two shapes, modified (multiplied) by dot product of the surface normals of the two correspondences.

Fig. 1 shows the superimposed liver shapes, from similar shape to dissimilar ones. Only rigid transformation is used for better visualization so the original shapes can be compared visually.

To quantitatively evaluate the performance of the proposed shape comparison, we use the Spearman's score that computes the rank correlation [20] on two of the shape similarity ranking orders. We get the Spearman's score on liver retrieval between

human operators and the method. As the liver shapes are highly complex, the shape similarity rank is quite subjective from person to person especially for dissimilar shapes comparison. Nevertheless, for those similar shapes, the rank should be consistent.

Here, the Spearman's score ρ between the two human operators is only *0.40*. Analyzing the result we found that for the dissimilar liver sets the retrieval results were quite subjective, which caused the low correlation among the sets. While for those liver shapes that have many similar samples, the correlation rank is higher, the score ρ=*0.53* if four sets that have less similarity with each other are not used in the comparison. The correlation score by using the CPD shape registration with the two human operators are increased to 0.54 and 0.47 respectively.

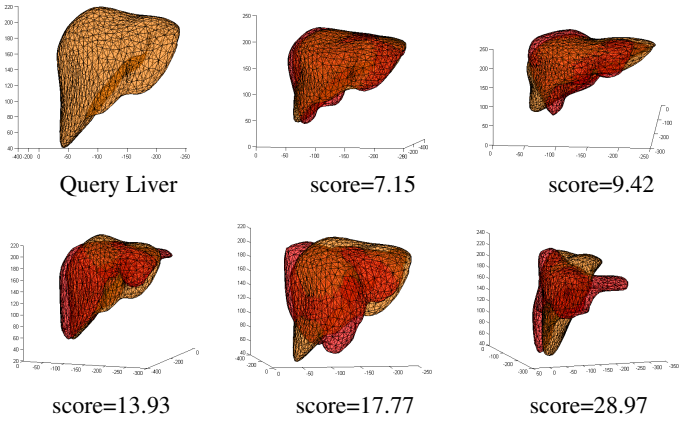

Fig. 1. Liver registration and score using modified mean Hausdorff distance measurement

2.2 Gallbladder Shape Modeling

GB shape can be intuitively and semantically represented by neck, size, orientation, and folds. To detect a GB fold, we use saliency region to segment a GB. We have developed a method for the decomposition [9]. However it has problems in ring-like saliency region caused by shape protrusion or large saliency region caused by a flattened fold. Here we present a new approach to find the proper cutting plane. With a surface mesh, a saliency region R_s at scale s is defined as a set of connected mesh vertices V, of which all the Gaussian curvatures K_s are negative due to the opposite values of the two principal curvatures.

$$R_s = \{v \in V,\ K_s(v) < 0\}. \tag{1}$$

To capture the global shape change, we detect all local minimum in R_s of Gaussian curvatures at largest scale N, $V_m = \{v_m \in V,\ K_N(v_m) < K_N(v_{r1}),\ v_{r1}$ is the neighboring vertices at ring 1 of $v_m\}$. As K_N is negative, we have

$$v_p = \arg\min_{v_m} K_N(v_m) C_m(v_m) . \tag{2}$$

The concavity C_m measures the minimum distance from the mesh vertex v_m to the mesh convex hull. It is a good measurement of the global shape concavity at the vertex. To consider the saliency region around v_p (2), set the curvature threshold as half of the local minima, $\xi_s=0.5K_s(v_p)$, $R_s = \{v \in V,\ K_s(v) < \xi_s\}$. A multiscale saliency region R_p is then defined as

$$R_p = \bigcup R_s, \text{ and } \bigcap R_s \neq \phi . \tag{3}$$

Let the saliency region be Q containing v_p. The center of the saliency region is the mean,

$$v_c = \frac{1}{N_Q} \sum_{v_i \in Q} v_i , \tag{4}$$

where Q has N_Q vertices. Define the main norm n_c for the saliency region as the surface norm nearest to v_c. The principal (curvature) directions of the surface at a vertex v_i in Q can be computed [19]. Shown in Fig. 2 are the curvature directions, with the blue lines being the minimum principal curvature directions p^n, and yellow lines being those for maximum principal direction p^m. Red dots are the saliency points forming the saliency region (on left image). Note that we are interested in a cutting plane aligned with n_c. Illustrated in Fig. 2 (central image), let the cutting plane have a normal n_p, v_c is a point on the plane, then $n_c \times n_p = 0$. Removing the n_c component from p^n, we have,

$$q^n = p_n - (p_n \cdot n_c) n_c . \tag{5}$$

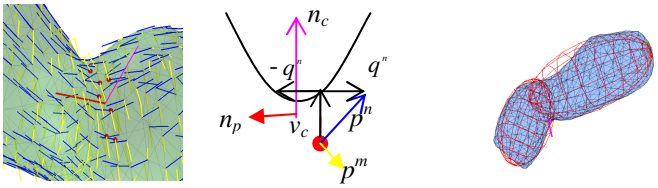

Fig. 2. Cutting plane using principal curvature direction. Left: partial surface at a saliency region, Middle: the illustration of the curvatures, Right: the ellipsoid fitting for a GB.

For a vertex, both p^n and $-p^n$ are possible depending on the surface property. Randomly select a q_0 we adjust the other direction q_i by aligning them with q_0,

$$q_i^n = \begin{cases} q_i^n, & if \quad q_i^n \cdot q_0^n >= 0 \\ -q_i^n, & if \quad q_i^n \cdot q_0^n < 0 \end{cases}. \tag{6}$$

The cutting plane normal is then computed as

$$n_p = \frac{1}{N_Q} \sum_i q_i^n . \tag{7}$$

With the cutting plane, the mesh vertices of a GB are separated into two sets of data points. One ellipsoid is applied to one set of points by the ellipsoid fitting.

The GB neck is further identified by a position related to the liver center. Let a GB mesh vertices be $G=\{g_i\}$, the liver mesh vertices be $L=\{l_j\}$, centered at l_c. The major principal axis O_g of G can be obtained by PCA. Mapping all $\{g_i\}$ to O_g, so $d_i= \{(g_i - g_c)\cdot O_g\}$. The GB neck N_e is obtained as one of the two extremes $\{g_{e1}=\arg\max(d_i), g_{e2}=\arg\min(d_i)\}$ that is close to the liver center l_c. Another extreme is taken as the fundus. Here, given N_e, a GB is simplified by the connection of the major axis of the decomposed ellipsoids, (E_1,E_2), pointing from the GB neck to the GB fundus. Fig. 3 illustrates such a GB topology, which is the semantic feature of the GB, written as $G = \{N_e,O_g,S_g,(E_1,E_2)\}$, where S_g is the size of the GB.

Depending on fold detection, a GB may have only one ellipsoid if no saliency region detected. For GBs A and B both with two ellipsoids (E^A_1,E^A_2), and (E^B_1,E^B_2), the bend difference (angle and size) is used to measure the similarity. By shifting N^A_e to N^B_e, and rotating the ellipsoids (E^A_1,E^A_2) around $E^A_1 \times E^B_1$ so that E^A_1 is aligned to E^B_1, the distance of the folds is,

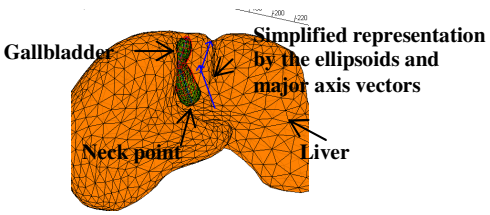

Fig. 3. Gallbladder representation

$$D_b = 1 - w_{AB} \frac{| E^A_2 \cdot E^B_2 |}{\| E^A_2 \| \times \| E^B_2 \|}. \tag{8}$$

The weight w_{AB} measures the difference of relative length I between the two folds,

$$w_{AB} = \min(\| I^A_1 \|, \| I^B_1 \|) / \max(\| I^A_1 \|, \| I^B_1 \|), \tag{9}$$

$$I^{G_1} = \| E^{G_1} \| / (\| E^{G_1} \| + \| E^{G_2} \|) . \tag{10}$$

If a GB G with only one ellipsoid E^G_1, letting $E^G_2 = E^G_1$, (8) still works well as a distance measurement. It can be shown that if the folds are the same, D_b=0.

2.3 Liver-Gallbladder Distance Measurement

In this study, liver volume is normalized so that it will not affect the comparison. It can always be added easily later whenever it is necessary. Mahalanobis distance is adopted to compute the joint liver-GB distance between patients, p_1 and p_2. Let D^L be the distance between liver shapes, and $D^G_{i=1,...,4} = (D_{N_e}, D_{O_g}, D_{S_g}, D_b)$ be the distance between the semantic features of the GBs. To balance the shape influence of liver and GB, the joint similarity is rewritten as

$$S(p_1,p_2) = 1 - \frac{1}{2}\left(\frac{|D^L|}{\sigma^L} + \frac{1}{4}\sum_i \frac{|D^G_i|}{\sigma^G_i}\right) . \tag{11}$$

The σ in (11) is the corresponding standard deviation.

3 Experiments and Result Analysis

Experiments have been conducted on a small data set including 19 liver-GB CT scans. Liver volume is normalized so that it will not affect the comparison. By visual examination of the results in Fig. 4, we can see that a high similarity score (11) does reflect the anatomical similarity, both in shapes and structures. The gallbladders are superimposed at the bottom-right for a better view. Query-1 has obtained very similar anatomical structures on top. Query 2 has only one similar instance, but due to the gallbladders' shapes are not similar, the overall score is low.

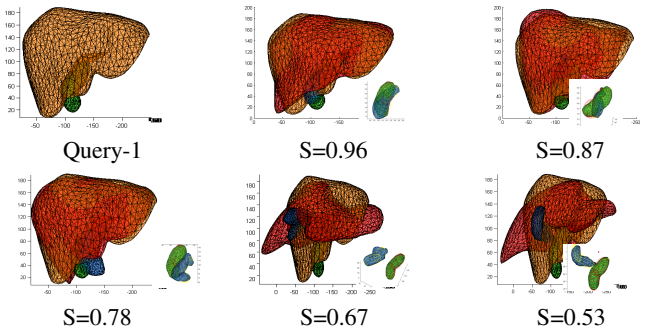

Fig. 4. Liver-GB retrieval with similarity scores

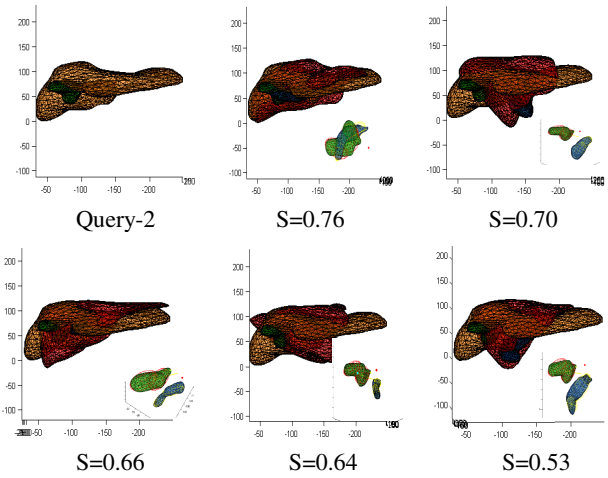

Fig. 4. (continued)

Spearman's rank correlation [20] is also used to measure the performance. The higher the Spearman's score ρ is, the more similar of the two ranks will be. Two users are asked to sort the data based on the visual similarity. The mean score ρ between the two users is 0.55, over all 19 queries. Compared with the results from the two users, the proposed approach got the mean scores ρ=0.50 and 0.40 respectively. The main difference is caused by some dissimilar datasets, which are difficult even for human operators to decide the similarity rank among them. If we take out the dissimilar sets (4 sets, irregular liver and gallbladder shapes), the score between the 2 operators is 0.68 and the scores go up to 0.64 and 0.54 between our method and the two human operators. We also tested the shape retrieval method in [21] using multi-view LightField Descriptor. Including all data for testing, the correlation score with human operators are 0.34 and 0.35. One of the reasons is that the LightField is good for similar objects, but it may not suitable for dissimilar objects. In GB comparison, the size and orientation are the factors to be considered, however which will be normalized by LightField.

4 Conclusion

This paper presents the approaches to model and compare 3D anatomical structures of liver-gallbladder pairs. Through jointly comparing the shape and structure features, the liver-gallbladder anatomical retrieval is developed. Although the data set collected and tested is small, it includes variant structures and shape changes like fundus fold, big fold in the middle of gallbladder, normal liver shapes, and abnormal liver shapes (some are due to lesions) with gallbladders in different types and positions. The

preliminary test shows that the approach successfully retrieved the data according to the similarities or dissimilarity. The quantitative results show that our method is highly correlated with human's performance.

The structure retrieval proposed in the paper is limited to either similar or dissimilar cases for the training purpose based on liver shape, GB shape and the relationship between liver and GB. The shape registration using CPD or other generic registration does not consider the semantic similarity of livers, such as the similarity between liver left/right lobes or the GB fossa shapes, which requires specific region identification on the lobes, segments and fossa. For GB comparison, only the biggest fold is detected and used for GB decomposition. For GBs with more complicated folds, the method may not be enough to characterize the shape variation. Currently the detected fold can be a real fold or a small 'fold' caused by the extension from GB to cystic duct. In the comparison (8), we do not distinguish the types of folds, but the relative length and position of the folds are used to measure the difference between two GBs.

Future works include the benchmark on more datasets, improvement using relevance feedback, and incorporation of other structures for data retrieval.

Acknowledgements. This project is funded by the Agency for Science, Technology and Research (A*STAR), Singapore under BEP Grant 1021480009.

References

1. Meilstrup, J.W., Hopper, K.D., Thieme, A.: Imaging of Gallbladder Variants. Am. J. Roentgenol. 157(6), 1205–1208 (1991)
2. Bodzioch, S.: Automated Detecting Symptoms of Selected Gallbladder Illness Based on A Static Ultrasound Images Analysis. Bio-Alg. and Med-Sys. 2, 35–44 (2006)
3. Kaiser, E.: Congenital and Acquired Changes in Gallbladder Form. Am. J. Dig. Dis. 6(7), 938–953 (1961)
4. Prasad, M.N., Brown, M.S., Ni, C., Margolis, D.J., Douek, M., Raman, S., Lu, D., Goldin, J.: Three-Dimensional Mapping of Gallbladder Wall Thickness on Computed Tomography Using Laplace's Equation. Acad. Radiol. 15, 1075–1081 (2008)
5. Xiong, W., Ong, S.H., Tian, Q., Xu, G., Zhou, J., Liu, J., Venkatash, S.K.: Construction of a Linear Unbiased Diffeomorphic Probabilistic Liver Atlas from CT Images. In: IEEE International Conference on Image Processing, pp. 1773–1776. IEEE Press, New York (2009)
6. Okada, T., Shimada, R., Sato, Y., Hori, M., Yokota, K., Nakamoto, M., Chen, Y.-W., Nakamura, H., Tamura, S.: Automated Segmentation of the Liver from 3D CT Images Using Probabilistic Atlas and Multi-level Statistical Shape Model. In: Ayache, N., Ourselin, S., Maeder, A. (eds.) MICCAI 2007, Part I. LNCS, vol. 4791, pp. 86–93. Springer, Heidelberg (2007)
7. Chi, Y., Cashman, P., Bello, F., Kitney, R.I.: An Automatic Liver Segmentation Initialization Information Retrieval Strategy for a Content-Based Image Retrieval System Followed by a New Liver Volume Segmentation Method for CT and MRI Image Datasets. In: MICCAI 2007 Workshop on Content-Based Image Retrieval for Biomedical Image Archives (2007)

8. Zhang, J., Huang, W., Zhou, J., Yang, T., Liu, J., Su, Y., Chui, C.K., Chang, S.: Gallbladder Modeling and Simulation in Laparoscopic Cholecystectom. In: IEEE International Conference on Industrial Electronics and Applications, pp. 128–131. IEEE Press, New York (2011)
9. Huang, W., Zhou, J., Liu, J., Zhang, J., Yang, T., Su, Y., Law, G.H., Chui, C.K., Chang, S.: 3D Shape Decomposition and Comparison for Gallbladder Modeling. In: Proc. of SPIE Medical Imaging, vol. 7964, p. 79642K (2011)
10. Tangelder, J.W.H., Veltkamp, R.C.: A Survey of Content Based 3D Shape Retrieval Methods. Multimed. Tools Appl. 39, 441–471 (2008)
11. Yamauchi, H., Gumhold, S., Zayer, R., Seidel, H.-P.: Mesh Segmentation Driven by Gaussian Curvature. Visual Comput. 2, 659–668 (2005)
12. Au, O.K.-C., Tai, C.-L., Chu, H.-K., Cohen-Or, D., Lee, T.-Y.: Skeleton Extraction by Mesh Contraction. J. ACM Trans. on Graphics 27(3), no. 44 (2008)
13. Myronenko, A., Song, X.: Point Set Registration: Coherent Point Drift. IEEE Trans. Pattern Anal. Mach. Intell. 32(12), 2262–2275 (2010)
14. Besl, P.J., McKay, N.D.: A Method for Registration of 3-D Shapes. IEEE Trans. Pattern Anal. Mach. Intell. 14(2), 239–256 (1992)
15. Shapira, L., Shamir, A., Cohen-Or, D.: Consistent Mesh Partitioning and Skeletonisation Using the Shape Diameter Function. Visual Comput. 24, 249–259 (2008)
16. Banegas, F., Jaeger, M., Michelucci, D., Roelens, M.: The Ellipsoidal Skeleton in Medical Applications. In: ACM Symposium on Solid Modeling and Applications, pp. 30–38 (2001)
17. Zhou, J., Xiong, W., Ding, F., Huang, W., Qi, T., Wang, Z., Oo, T., Venkatesh, S.K.: Liver Workbench: A Tool Suite for Liver and Liver Tumor Segmentation and Modeling. In: Loménie, N., Racoceanu, D., Gouaillard, A. (eds.) Advances in Bio-imaging. AISC, vol. 120, pp. 193–207. Springer, Heidelberg (2012)
18. Su, Y., Chua, K.S., Chong, C.S.: Mesh Processing Using Virtual Geometry. WSEAS Transactions on Computers 5(4), 696–704 (2006)
19. Cohen-Steiner, D., Morvan, J.-M.: Restricted Delaunay Triangulations and Normal Cycle. In: ACM Symposium on Computational Geometry, pp. 237–246 (2003)
20. Vogel, J., Schiele, B.: Semantic Modeling of Natural Scenes for Content-Based Image Retrieval. Int. J. Comput. Vis. 72(2), 133–157 (2007)
21. Chen, D.-Y., Tian, X.-P., Shen, Y.-T., Ouhyoung, M.: On Visual Similarity Based 3D Model Retrieval. In: Computer Graphics Forum (EUROGRAPHICS 2003), vol. 22(3) (2003)